CHARACTERISATION OF THE THERMAL RESPONSE OF A LI-ION BATTERY MODULE TO TRANSIENT LOADS – A NUMERICAL STUDY

Saeed A.[1]*, Karimi N.[1,2], Paul M[1].
[1]James Watt School of Engineering, University of Glasgow, Glasgow G12 8QQ, United Kingdom
[2]School of Engineering and Materials Science, Queen Mary University of London, London E1 4NS, United Kingdom
*Author for correspondence
E-mail: a.saeed.1@research.gla.ac.uk

ABSTRACT

Li-ion batteries are known to be highly sensitive to operational temperatures and exceeding a narrow range of temperature can damage them permanently. So far, most research efforts on battery thermal management considered steady conditions. However, in practice, battery heat generation is proportional to the load, which is highly time dependent. Hence, batteries often experience a transient change of temperature, turning battery cooling into a time-dependent problem. An essential step in tackling such problem is characterisation of the thermal response of battery to different transient loads. To achieve this, the electric loads, acting on the battery, are inferred from the standard driving cycles and their required mechanical power. Also, a numerical model for cooling of a battery module is developed using OpenFoam. Thermal response of the system is then simulated for different driving scenarios. Particular attention is paid to the steeply increasing loads, as they can be potentially more harmful to batteries. The results show that during transient loading, the instantaneous temperature of some battery cells in the module could significantly exceed the safe limits. The effects of type and velocity of the coolant and the location of a cell in the module, upon the temperature traces of the cell are discussed.

INTRODUCTION

Hybrid Electric Vehicles (HEV) and Electric Vehicles (EV) have gained enormous attention due to significant worldwide efforts to combat rising environmental concerns and reduce greenhouse gas emissions [1]. However, finding energy storage solutions capable of quick charging, high mileage and high performance remains one of the biggest challenges facing EVs [2]. Lithium-ion (Li-ion) batteries have gained notable attention for use as energy storage within EVs due to their high energy density, lightweight, prolonged life cycle, low self-discharge rate and recyclability compared to their nickel-metal or lead-based counterparts [3]. Nevertheless, these batteries' operating safety and performance – life cycle, discharge capacity – are heavily dependent on the operational temperature [4–6]. Hence, effective battery temperature control has become crucial for battery thermal management systems (BTMS) in EVs.

Studies by Kim et al. [7] and Suh et al. [8] have shown that to sustain a healthy and safe operating electrochemical rate of reaction., the battery cell temperatures should stay between 25°C and 45°C. Further, the cell-to-cell temperature difference should not exceed 5°C. Due to their complex and relatively unstable chemistry, excessively high or low temperatures can lead to electrolyte decomposition causing irreversible damage to the battery cell and shortening its lifetime [9,10]. Moreover, this can worsen when hundreds or thousands of battery cells are connected in series, parallel or series-parallel. Long term existence of large cell to cell temperature differences can create hot spots within a battery module, altering its charging and discharging capabilities. The uneven temperature distribution across the battery module can lead to poor consistency within a battery pack, further leading to each battery cell displaying a variety of thermal effects.

NOMENCLATURE

H	(m)	Height
L	(m)	Single Cell Section Length
Nu	(-)	Nusselt Number
Re	(-)	Reynolds Number
R	(m)	Radius

Degradation of a single cell within a battery module weakens its performance – the weakest cell may determine the performance characteristics of the battery pack. This further amplifies the cell-by-cell temperature difference, creating a vicious cycle [9]. Therefore, to combat extreme temperatures and maximise the battery pack lifetime, many BTMS have been studied, from forced air and water-cooling to phase change materials and heat pipes as passive cooling [10,11]. However, designing such systems requires extensive knowledge of internal heat generation, thermal transport, and heat dissipation mechanisms. Moreover, due to the highly complex and dynamic nature of heat transfer in Li-ion batteries, time-dependent thermal management systems are a present issue [10,12]. Most studies have primarily focused on understanding the dynamics of heat generation under steady loads, whereas only a few studies have investigated the heat transfer of Li-ion batteries under dynamic loads.

In a previous investigation, Yang et al. [13] numerically compared the effects of aligned and staggered arrangements of battery cells using a 2D conjugate heat transfer model with a 1D electrochemical model. The study focused on optimising the longitudinal and transverse spacing between cells. It was found that the aligned battery cell arrangement led to far greater temperature uniformity. However, the staggered arrangement led to an overall cooler battery pack. Further, increasing the transverse gap between cells in the aligned battery module dominated the heat transfer efficiency, requiring a much larger

battery module. Therefore, for a densely packed battery module, the gaps between each cell need to be kept at a minimum without compromising thermal efficiency.

Most existing thermal battery management systems studies are primarily concerned with evaluating the flow field and heat generation inside battery cells under steady flow conditions. This demands extensive use of computational power to determine the battery thermal behaviour accurately. However, due to the dynamic nature of driving, steady models for evaluating the thermal response are not compatible. This paper aims to fill this gap by using computational modelling of unsteady internal heat generation inside battery cells using real-time driving data. The corresponding dynamic response of heat convection is then analysed to determine the effectiveness of the BTMS under extreme driving scenarios.

PROBLEM CONFIGURATION

A general sketch of a battery pack module, the simulated model and a two-dimensional schematic of a single cell section can be seen in figures 1a, 1b and 1c, respectively. The battery cells are arranged in a staggered cell configuration containing six primary cells. A single cell section has a length, L, of 100mm [14], height, H, of 50mm [14], and a depth, D, of 100mm [14]. Each battery cell has a radius, R, of 20mm [14].

NUMERICAL METHODS

An unsteady, three-dimensional computational fluid dynamics (CFD) model was developed to investigate the thermal response of the system to unsteady modulations in the internal heat generation of each battery cell. A grid independency check was also carried out on the computational model to minimise computational costs while maintaining a high level of accuracy.

Under steady-state conditions, the internal heat generation of the battery was assumed to be 2000 W/m^3. This value was chosen to represent a running car's battery and fluid temperature prior to introducing a large acceleration. Further, this value was calculated using the current model geometry, average Li-ion cell efficiency of 85% and the 85 kW battery specifications of the Tesla Model S [15]. In comparison to fluids like water, air has low thermal conductivity; therefore, high inlet velocities are required to sufficiently cool down the battery pack using air. Therefore, the inlet Reynolds number for air was calculated to be 44,000. Whereas for water, the inlet Reynolds number was 2,300.

The numerical simulations were conducted using an open-source, finite-volume method based CFD software called OpenFOAM v2006. A conjugate heat transfer model called chtMultiRegionFoam was used to accurately study conduction within each battery cell due to internal heat generation and convection to the fluid. A k-ε turbulence model is utilised to accurately model and solve the flow field of the coolant fluid. The differences between the two chosen coolant fluids require the use of different models – for air, an ideal gas model is employed, whereas for water, a constant density model is used. The time-step is chosen to be five orders of magnitude smaller than the full timescale to accurately model vortex shedding. Further, all models use a second-order discretisation scheme for added accuracy.

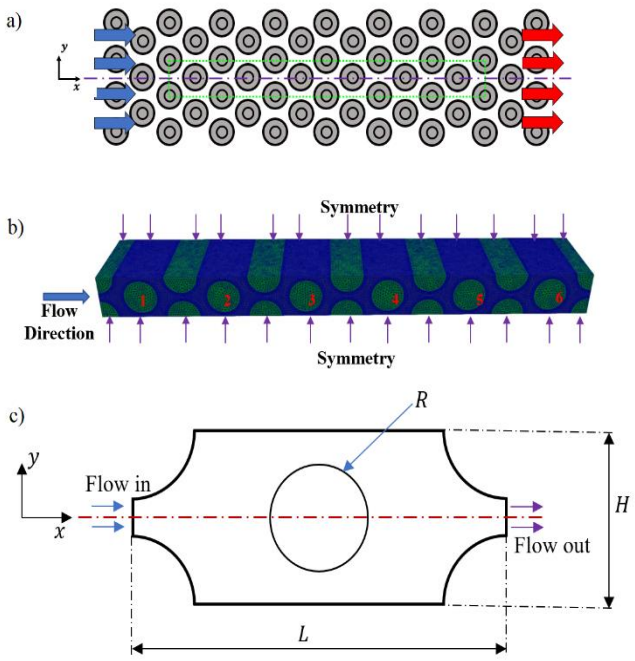

Figure 1 – a) Battery pack module, b) Simulation model and c) 2D schematic of a single cell section.

Internal combustion vehicles emit a range of atmospheric pollutants which have to be regulated. However, exhaust emissions are inherently unpredictable unless they can be reproduced under standardised laboratory conditions known as standard dynamometer drive cycles. Three drive cycles are chosen for this study. The first drive cycle is the New York City cycle (NYCC), featuring low speed, stop-and-go traffic conditions for inner-city travel. Next is the SC03 drive cycle, also known as the Supplemental Federal Test Procedure (FTP) driving schedule. Finally, the Under Dynamometer Driving Schedule (UDDS) is the city test. The United States Environmental Protection Agency uses the drive cycles mentioned before as part of its emissions testing kit.

Validation

The present study was validated against experimental and numerical data. The validation data for air and water can be seen in Tables 2, 3 and 4, respectively. During validation, the model parameters are modified so that the flow occurs over a single cylinder. The input parameters for the single-cylinder validation study can be seen in Table 1.

Table 1 – Single-cylinder validation input parameters

Ambient fluid temperature (T_∞)	300 K
Cylinder Surface Temperature (T_s)	700 K
Cylinder radius (R)	0.02 m
Air density (ρ)	1.1614 kg/m^3
Air dynamic viscosity (μ)	1.846e-05 kg/ms
Air thermal conductivity (k)	0.02624 W/mK
Water density (ρ)	996.53 kg/m^3
Water dynamic viscosity (μ)	8.65e-04 kg/ms
Water thermal conductivity (k)	0.59783 W/mK

The comparison of the air model against the Churchill and Bernstein [16] correlation can be seen in Table 2. At values of Reynolds number where a laminar condition can be assumed, the simulated data and both correlations show minimal differences. However, as the value of Re is increased, the error also increases, with the max error being 7.34% at a Re of 20,000.

Table 2 – Comparison of the numerical simulations with correlation from literature for air – Single cylinder

Re	50	150	1,000	3,900	10,000	20,000
Nu	3.78	6.28	14.98	31.09	55.792	84.990
Churchill and Bernstein [16] correlation						
	3.74	6.28	15.99	32.45	53.540	79.177
Error (%)	1.12	0.05	6.36	4.18	4.21	7.34

Moreover, to evaluate the solver's unsteady performance, the current model without battery cells is exposed to ramp disturbances in the flow temperature at an Re value of 180. The changes in the flow temperature at different locations along the domain are compared to direct numerical simulation (DNS) data by Christodoulou et al. [17]. The largest error was found to be less than 1.4%.

Table 3 – Comparison of the numerical simulations with correlations from literature for water – Single cylinder

Re	50	150	1,000	4,000	10,000
Nu	8.525	14.99	41.091	86.262	144.44
Churchill and Bernstein [16] correlation					
	8.756	14.88	39.233	82.607	139.69
Error (%)	2.64	0.74	4.73	4.42	3.48

The single-cylinder simulated model against the Churchill and Bernstein [16] correlation and experimental data by Stephen Whitaker [18] can be seen in Tables 3 and 4. As previously stated, at low values of Re, the simulated Nusselt number and the correlation are in good agreement. However, as the value of Re increases, so does the error. The correlation shown in Table 3 shows that the most significant error is 4.73% at a Re value of 1,000. Furthermore, compared against the experimental data, the largest error is 3.015% at an Re of 2,000.

Table 4 – Comparison of the numerical simulations with the experimental data from literature for water – Single cylinder

Reynolds Number	50	150	2,000
Simulated Nu	8.525	14.99	62.08
Stephen Whitaker	8.560	15.33	64.01
Error (%)	0.409	2.218	3.015

The excellent agreement of the numerical and experimental data and DNS data for air and water confirms the validity of the numerical analysis presented in this study.

RESULTS AND DISCUSSION

In this section, the battery cells' response to unsteady modulation is presented. It should be noted that during analysis, the average battery cell surface temperatures are discussed. The Reynolds number is kept constant since the flow field is not modulated. Therefore, it can be argued that there would be minuscule changes in the Nusselt number by modulating the battery cell's internal heat generation. This results in a more effective comparison of the coolant fluids, drive cycles, and whether the battery cells' temperatures remain within the optimal range. Additionally, the settling time and maximum overshoot are also calculated to determine the system's responsiveness. Where the former is described as the time needed for a system to reach and stay within two percent of the final value. The maximum overshoot is defined as the comparison of the peak and the desired value of the system. For the sake of brevity, only the NYCC and UDDS drive cycles are discussed.

Figure 2 shows the spatiotemporal response of the temperature field to a linear ramp in the internal heat generation using the NYCC drive cycle. The steady-state temperature field prior to introducing a ramp is shown in figure 2a. Due to a small internal heat generation value, the fluid and battery cells' temperatures are almost indistinguishable. However, shortly after the ramp begins, the battery cells begin to heat up, and a clear difference in the fluid and battery cell temperatures can be seen. Figure 2c and 2d show the temperature fluid before reaching the new steady-state condition and once the model has reached equilibrium, respectively. As the fluid flows downstream, it begins to reach the temperature of the battery cells, showcasing a typical convective system.

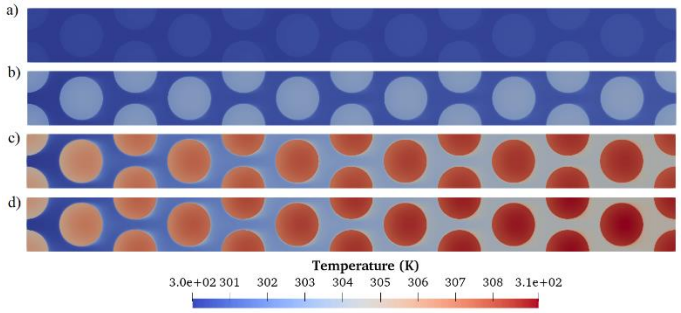

Figure 2 – Spatiotemporal evolution of the temperature field using NYCC drive cycle with water as the inlet fluid. Where a) is before the ramp, b) 25s after the ramp begins, c) 100s before reaching equilibrium and d) At equilibrium.

Figure 3a and 3b depict the temporal response of the battery cell surface temperatures to internal heat generation ramps based on the NYCC and UDDS drive cycles with air as the coolant fluid, respectively. Using the speed-time data given by the NYCC drive cycle, one of the largest accelerations were found to produce a ramp with a lower limit of 2000 W/m^3 and an upper limit of 15,582 W/m^3 with a duration of 23 seconds. It should be

noted that each simulation was allowed to run for 15 seconds prior to introducing the ramps. Through visual inspection of figure 3a, it can be very clearly seen that the average surface temperature of each battery cell continued to rise even after the ramp was completed. Cell one starts at a temperature of 301.3 K and reaches a peak of 303.9 K before decreasing and reaching a steady-state value of 303.8 K; an overall temperature increase of 2.5 K with a maximum overshoot of 0.1 K. However, cell six starts at 309.3 K, reaching a maximum value of 312 K before becoming steady at 311.9 K. This leads to an overall temperature increase of 2.6 K with a maximum overshoot of 0.1 K. In addition, the settling time of each battery cell increases as you go further downstream. This is to say that for cell one to reach two percent of the final value takes 76.9 seconds, whereas for cell six to reach two percent of the final value takes 86.2 seconds once the ramp starts.

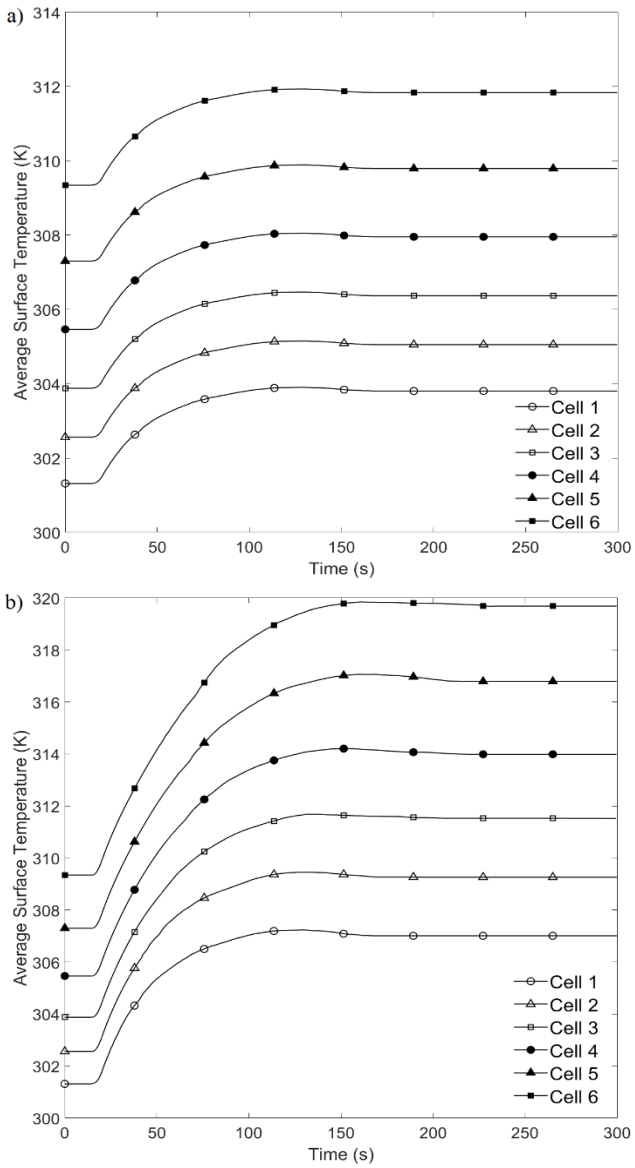

Figure 3 – Average battery cell surface temperature with air as the inlet fluid a) NYCC and b) UDDS.

Furthermore, a larger and steeper ramp is found using the UDDS drive cycle data. This results in a ramp with a starting value of 2000 W/m^3 and a maximum value of 37,990 W/m^3 in 7 seconds. This means that the UDDS ramp has to increase by over 2.4 times in less than three times the duration leading to steeper and overall more significant temperature increases, as seen in figure 3b. As expected with any convective system, the battery cells closer to the outlet experience a far higher temperature rise than those at the inlet. This is due to the increase in the coolant fluid temperature as it travels further downstream. Cell one starts at the same pre-ramp temperature and rises to a maximum temperature of 307.2 K before decreasing and reaching equilibrium at 307 K. This results in a total temperature increase of 5.8 K and a maximum overshoot of 0.2 K. Cell six rises to a maximum temperature of 319.9 K and then decreases to a steady-state value of 319.5 K. This leads to an overall temperature rise of 10.2 K and a maximum overshoot of 0.4 K. Comparing the temperature differences between the two drive cycles leads to no obvious correlation. This is to say that increasing the upper limit of the ramp by 2.4 times does not result in the overall temperature increase to also increase by this ratio. The ratio of temperature increases between the two drive cycles for cell one is 2.3, whereas, for cell six, the ratio is 3.9. Further, the trend of an increasing settling time further downstream can also be seen in figure 3b. However, due to the large internal heat generation ramp within a short, a considerably larger settling time is needed. Cell one takes 80.2 seconds to reach within two percent of the final value. Whereas for cell six to reach the same condition takes 125.7 seconds once the ramp begins.

Moreover, the internal battery cell temperatures are also measured to determine if the battery cells are kept within the safe operating range. Twenty-five probes are used along the y-axis in the centre of each battery cell. The temperature reported by these probes is then averaged for each time step. The resultant graphs can be seen in figure 4, where figures 4a and 4b show the average internal battery temperatures for the NYCC and UDDS drive cycles, respectively. The cell-to-cell differences prior to introducing the ramp are already out with the 5^{o}C limit. However, this difference is further intensified after the ramp is finished. For the NYCC drive cycle, the maximum starting cell-to-cell difference is 8.5 K, whereas, once each battery cell reaches equilibrium, this value increased to 8.9 K. Due to the larger internal heat generation for the UDDS drive cycle, the maximum cell-to-cell temperature difference is far higher at 13.8 K, an increase of over 60% as compared to the starting cell-to-cell temperature difference.

The temporal response of the UDDS drive cycle to internal heat generation on each battery cell with water being the inlet fluid can be seen in figure 5, where figure 5a and 5b show the average battery surface and battery internal temperature respectively. The drastic differences between figures 3a, 3b, and 5a are due to the two coolant fluids having significantly different thermophysical properties. The general trend in both figures is a temperature increase in all battery cells. However, unlike the figures shown for air, the water results show no sign of an overshoot. This can be accredited to the fact that water has a far higher specific heat capacity and thermal conductivity than air. This is also why the water results start at a significantly lower

temperature with minimal differences between each battery cell. Due to the NYCC drive cycle producing a menial temperature rise, no further NYCC drive cycle results are presented.

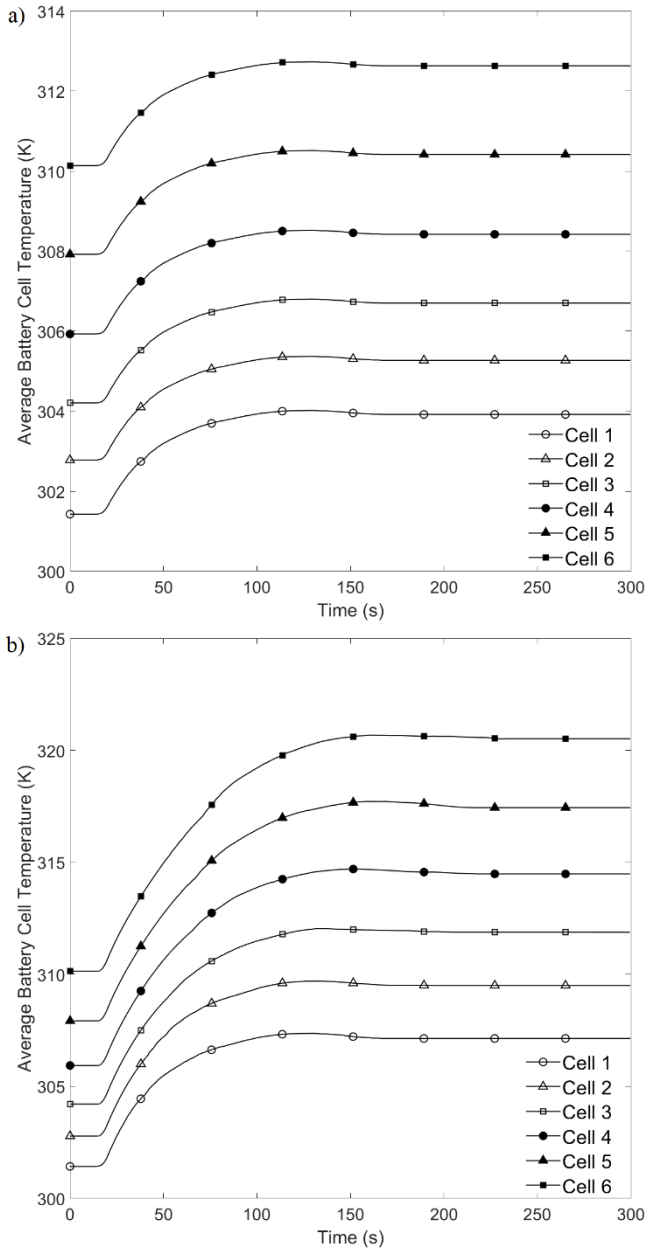

Figure 4 – Average battery internal temperature due to with air as the inlet fluid a) NYCC and b) UDDS.

A lower overall temperature rise for all battery cells can be seen in figure 5a, which uses the same ramp condition as figure 4b. Cell one starts at an average surface temperature of 300.2 K and rises to a maximum of 303.8 K, leading to an overall temperature rise of 3.6 K. Further, cell six starts at a temperature of 300.4 K and reaches a maximum temperature of 307.5 K, an overall increase of 7.1 K. Moreover, water is significantly more effective at removing heat and the resultant no overshoot leads to far shorter settling times compared to those seen when the coolant fluid is air. Cell one reaches two percent of the final value 77.7 seconds, whereas cell six reaches the same condition in 115.4 seconds once the ramp begins.

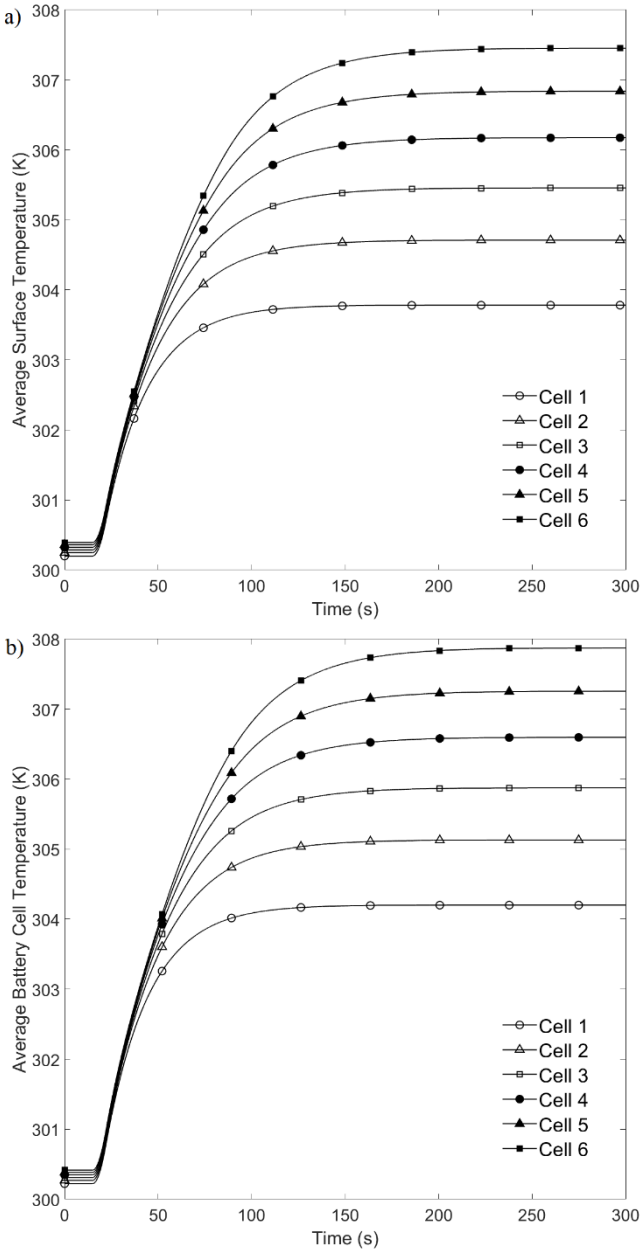

Figure 5 – Battery cell temperatures using the UDDS drive cycle with a) Average surface and b) Average internal battery temperature.

As anticipated, comparing the two responses from figures 3b and 5a, water as the coolant fluid is more successful at achieving low temperatures and becoming steady. This means that using water as the inlet fluid would reduce the overall temperature increase by almost 40%. At the same time, the steady-state condition is reached over 8% faster. Furthermore, as previously mentioned, the optimal operating range for a Li-ion battery is between 298 K and 318 K while maintaining a maximum cell-

to-cell temperature difference of 5 K. The cases with water can achieve these conditions. In contrast, the cases with air show a significant temperature difference between each cell. However, apart from cell six in figure 6b, all cells are kept within safe margins. The differences between the temperature increases, settling, and response time or air and water-cooled systems are related to the difference in their thermophysical properties, particularly the Prandtl number. At fixed values of Re, lower Prandtl numbers, such as those of air, can hinder efficient convective heat transfer.

CONCLUSION

Electric Vehicles have been given a spotlight as a potential counter to the ever-growing concerns of global warming. However, one of the biggest issues facing EVs is their battery performance, which is directly coupled with its operating conditions. The temperature of each battery cell is determined by a wide array of driving patterns and vehicle operation. Therefore, thermal management of battery cells requires accurately predicting their temperatures during operation, which can be straightforward for systems with constant parameters. However, such parameters are a rare occurrence for vehicle driving scenarios. Three drive cycles were analysed to determine points at which the battery cells would be under extremes stress, such as high acceleration in a short period. The conditions were presented as ramps during numerical modelling, and the corresponding temperatures were analysed for two different coolant fluids. The cases with air resulted in high overall temperature increases, with an overshoot being present for all battery cells. In particular, the temperatures always exceeded the maximum cell-to-cell limit, and in the case of UDDS, cell six fell out of bound for the maximum safe operating temperature. In comparison, all cases with water remained within optimal operating ranges. Additionally, small maximum overshoots are noticed in large period ramps, such as the NYCC data. This is due to better completion of the fluid dynamics and transport interactions, allowing the fluid to accommodate for changes in the battery surface temperature effectively.

REFERENCES

[1] Xia, G., Cao, L. and Bi, G., 2017. "A review on battery thermal management in electric vehicle application". *Journal of Power Sources*. p. 90–105. https://doi.org/10.1016/j.jpowsour.2017.09.046

[2] Lukic, S.M., Cao, J., Bansal, R.C., Rodriguez, F. and Emadi, A., 2008. "Energy storage systems for automotive applications". *IEEE Transactions on Industrial Electronics*. p. 2258–67. https://doi.org/10.1109/TIE.2008.918390

[3] Kim, T.H., Park, J.S., Chang, S.K., Choi, S., Ryu, J.H. and Song, H.K., 2012. "The current move of lithium ion batteries towards the next phase [Internet]". *Advanced Energy Materials*. p. 860–72. https://doi.org/10.1002/aenm.201200028

[4] Vetter, J., Novák, P., Wagner, M.R., Veit, C., Möller, K.C., Besenhard, J.O., Winter, M., Wohlfahrt-Mehrens, M., Vogler, C. and Hammouche, A., 2005. "Ageing mechanisms in lithium-ion batteries". *Journal of Power Sources*, 147(1–2), pp. 269–81. https://doi.org/10.1016/j.jpowsour.2005.01.006

[5] Ma, Y., Mou, H. and Zhao, H., 2020. "Cooling optimization strategy for lithium-ion batteries based on triple-step nonlinear method". *Energy*, 201pp. 117678. https://doi.org/10.1016/j.energy.2020.117678

[6] Bandhauer, T.M., Garimella, S. and Fuller, T.F., 2011. "A Critical Review of Thermal Issues in Lithium-Ion Batteries". *Journal of The Electrochemical Society*, 158(3), pp. R1. https://doi.org/10.1149/1.3515880

[7] Kim, H., Park, S.G., Jung, B., Hwang, J. and Kim, W., 2013. "New device architecture of a thermoelectric energy conversion for recovering low-quality heat". *Applied Physics A 2013 114:4*, 114(4), pp. 1201–8. https://doi.org/10.1007/S00339-013-7844-7

[8] Suh, I.S., Cho, H. and Lee, M., 2014. "Feasibility study on thermoelectric device to energy storage system of an electric vehicle". *Energy*, 76pp. 436–44. https://doi.org/10.1016/J.ENERGY.2014.08.040

[9] An, K., Barai, P., Smith, K. and Mukherjee, P.P., 2014. "Probing the Thermal Implications in Mechanical Degradation of Lithium-Ion Battery Electrodes". *Journal of The Electrochemical Society*, 161(6), pp. A1058–70. https://doi.org/10.1149/2.069406jes

[10] Wang, H., He, F. and Ma, L., 2016. "Experimental and modeling study of controller-based thermal management of battery modules under dynamic loads". *International Journal of Heat and Mass Transfer*, 103pp. 154–64. https://doi.org/10.1016/j.ijheatmasstransfer.2016.07.041

[11] Zhao, R., Zhang, S., Liu, J. and Gu, J., 2015. "A review of thermal performance improving methods of lithium ion battery: Electrode modification and thermal management system". *Journal of Power Sources*. p. 557–77. https://doi.org/10.1016/j.jpowsour.2015.09.001

[12] Li, X., He, F. and Ma, L., 2013. "Thermal management of cylindrical batteries investigated using wind tunnel testing and computational fluid dynamics simulation". *Journal of Power Sources*, 238pp. 395–402. https://doi.org/10.1016/j.jpowsour.2013.04.073

[13] Yang, N., Zhang, X., Li, G. and Hua, D., 2015. "Assessment of the forced air-cooling performance for cylindrical lithium-ion battery packs: A comparative analysis between aligned and staggered cell arrangements". *Applied Thermal Engineering*, 80pp. 55–65. https://doi.org/10.1016/j.applthermaleng.2015.01.049

[14] Mahamud, R. and Park, C., 2011. "Reciprocating air flow for Li-ion battery thermal management to improve temperature uniformity". *Journal of Power Sources*, 196(13), pp. 5685–96. https://doi.org/10.1016/j.jpowsour.2011.02.076

[15] Tesla Motors Patent US 8286743., 2012. "Vehicle battery pack ballistic shield [Internet]". p. Patent US 8286743.

[16] Churchill, S.W. and Bernstein, M., 1977. "A correlating equation for forced convection from gases and liquids to a circular cylinder in crossflow". *Journal of Heat Transfer*, 99(2), pp. 300–6. https://doi.org/10.1115/1.3450685

[17] Christodoulou, L., Karimi, N., Cammarano, A., Paul, M. and Navarro-Martinez, S., 2020. "State prediction of an entropy wave advecting through a turbulent channel flow". *Journal of Fluid Mechanics*, 882. https://doi.org/10.1017/JFM.2019.799

[18] Whitaker, S., 1972. "Forced convection heat transfer correlations for flow in pipes, past flat plates, single cylinders, single spheres, and for flow in packed beds and tube bundles". *AIChE Journal*, 18(2), pp. 361–71. https://doi.org/10.1002/aic.690180219